

Signal Processing for Integrated, High Performance, Low Noise Chemical/Biological Sensor Interface

Drago Strle, Janez Trontelj

University of Ljubljana, Faculty for Electrical Engineering, Ljubljana, Slovenia

Abstract: The article presents miniature detection system and its associated signal processing electronics, which can detect and selectively recognize vapor traces of different materials including explosives. It is based on surface-functionalized COMB capacitive sensors and extremely low noise analog integrated electronic circuit, hard-wired digital signal processing and additional software running on the PC. The instrument is sensitive and selective, consumes minimum amount of energy, is very small (few mm³) and cheap to produce in large quantities, and is insensitive to mechanical influences. Using electronic detection system built of low noise analog front-end and hard-wired digital signal processing, it is possible to detect less than 3ppt of TNT molecules in the atmosphere (3 TNT molecules in 10¹² molecules of the air) at 25 °C in 1 Hz bandwidth using very small volume and approx. 10 mA current from 5 V supply voltage. The sensor is implemented in modified MEMS process and analog electronics in 0.25 um CMOS technology.

Keywords: Chemical/Biological Sensor interface, Low noise signal processing, high performance integrated sensors

Signalno procesiranje za integriran, visokozmogljiv nizkošumni vmesnik za kemijske/biološke senzorje

Izvleček: Članek predstavlja miniaturni detekcijski sistem in pripadajoče integrirano elektronsko vezje, ki selektivno zaznava pare različnih materialov vključno s parami eksplozivov. Bazira na površinsko modificiranih COMB kapacitivnih senzorjih in nizkošumnem analognem integriranem vezju, skupaj z digitalnim procesorjem signalov in programsko opremo na PC računalniku. Instrument je zelo občutljiv, selektiven, porabi malo električne energije za svoje delovanje, je zelo majhen (nekaj mm³), je neobčutljiv na mehanične in temperaturne vplive in ga je mogoče ceneno proizvajati v velikih količinah. Z uporabo predstavljenega nizkošumnega procesiranja signalov je mogoče zaznati manj kot 3 TNT molekule v 10¹² molekulah nosilnega plina ali v atmosferi pri 25 °C in v 1 Hz pasovne širine. Instrument ima majhen volumen ter porabi približno 10 mA toka pri napajanju 5 V. Senzor je izdelan v modificiranem MEMS procesu, analogni del elektronike pa v 0.25 um CMOS procesu.

Ključne besede: kemijski/biološki sezorski vmesniki, nizkošumno procesiranje signalov, visoko občutljivi integrirani senzorji

* Corresponding Author's e-mail: drago.strle@fe.uni-lj.si

1 Introduction

Detecting vapor traces of different materials including explosives in the atmosphere is a potentially powerful method to reveal the presence of different toxic materials, explosives and land mines. The principle of detection method is based on the fact that most materials, including explosive devices, constantly emit rather small, but detectable number of different molecules, constituting the material. Numerous detection systems on the market are capable of detecting vapor traces of explosives

[1]. Their common limitations are rather large size, high power consumption, unreliable detection with false alarms, insufficient sensitivity and chemical selectivity or hypersensitivity to mechanical influences, long time needed for detection and extremely high price.

Currently, the most popular method for detection of vapor traces of target molecules is the chemo-mechanical sensor system based on cantilever bending, caused by adsorption of target molecules on asymmetrically modified surface. Bending is measured with optical

or electrical detection [2]. Optical cantilever position measurements are difficult; the apparatus is bulky and sensitive to the environmental influences like temperature, vibrations, pressure etc.; the integration and miniaturization is not possible. In this work, we present the detection system that measures the change of the capacitance caused by adsorption of target molecules to the surface of functionalized miniature MEMS capacitors with fixed COMB fingers; the environmental problems described above for the cantilever based sensors are completely eliminated. The adsorption of target molecules on functionalized surfaces of the fixed COMB capacitors causes the change of the dielectric constant of the monolayer between the plates of the capacitor. This extremely small change can be measured with extremely sensitive electronic measurement system described in this article.

The paper is organized as follows. In section 2, the principles of operation of the capacitive COMB sensor is shortly described to understand the requirements for the electronic measurement system. Section 3 deals with system design and modeling issues, while section 4 presents most important circuit design steps together with sensitivity estimates. Section 5 describes high level modeling and simulation results of the circuit which includes analog, mixed signal and digital modules. Section 6, presents responses of the detection system to the TNT and RDX vapors, the detection limits are calculated and compared to the estimates from the system level simulation results. Measured results are compared to the state of the art detection systems.

2 Sensor operation

The detection measurement system is composed of four differently functionalized differential COMB capacitive sensors (Fig. 1) connected to one channel of the low-noise analog electronic measurement system, followed by the DSP as presented on Fig. 2.

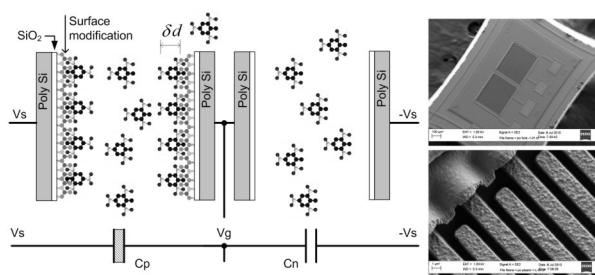


Figure 1: Comb capacitive sensor implemented in 1 μ m MEMS process: (Left) COMB capacitance change due to adsorption of the target molecule in the air. (Right) SEM micrograph of a differential COMB capacitor and the detail of its structure.

The principle of sensor operation is presented on the left part of Fig. 1. Each sensor is composed of a pair of COMB capacitors implemented in modified MEMS technology (SEM micrograph is shown on the right side of Fig. 1), where the fingers are not released from the bottom oxide. Both capacitors are covered with approx. 15 nm of silicon dioxide [3]. One capacitor in each pair is chemically functionalized with different organosilanes (APS, APhS or UPS) [4] to [5], as shown symbolically on the left part of Fig. 1 (shaded symbol of functionalised capacitors). For example, C_p is modified while C_n is not. During operation, on average, approx. equal numbers of target molecules are present in the space between the plates of both capacitors. Other molecules are also present in the air around both sensors; again, the density of all the molecules is on average distributed equally between capacitors and the capacitance difference is the same. The target molecules adsorb preferentially [7] to the surface of the C_p and change the relative dielectric constant between the plates, while C_n remains the same. Using differential excitation signal V_s , connected to both capacitors, one can measure the difference of the two capacitances caused by adsorbed target molecules. Each capacitor consists of 50 fingers with length of 350 μ m, height of 2 μ m and the distance between the fingers of approximately 1.5 μ m, thus forming two capacitors, each having a capacitance of approximately 0.4 pF with matching accuracy better than 5%, which is reduced by automatic calibration procedure before every measurement. At the moment, each differential sensor is produced and functionalized individually, while the modification layer is removed from one half of each differential pair using laser erosion procedure. In the near future, we plan to build an array of differently and selectively modified sensors on top of the ASIC chip to reduce the parasitic effects caused by bond-wires and parasitic capacitances and thus to increase the sensitivity.

3 Measurement system

Fig. 2 shows simplified block diagram of the sensor measurement system that includes low-noise analog signal processing electronics implemented in 0.25 μ m CMOS process together with four differently modified sensors, one channel of remaining analog signal processing electronics (AFE) and the digital signal processing block (DSP) in the gray area of Fig. 2. The DSP is currently implemented on the FPGA but in the future it will be implemented on-chip. The system architecture is in fact a multi-frequency lock-in amplifier where necessary part of the signal processing happens in the block of analog signal processing (AFE) and the rest using digital signal processing (DSP). The AFE consists of minimum amount of necessary analog electronics to

convert extremely weak capacitive changes to the digital stream. The AFE is programmable in many ways, so it can be adapted to different signal levels, frequencies, sensors etc. Each sensor is driven by a high frequency differential square-wave signal V_{s_i} with slightly different and adjustable frequency and amplitude. The capacitors of the first sensor are driven with differential square-wave signal V_{s_1} with frequency f_{s_1} , the capacitors of the second sensor are driven with differential square-wave signal V_{s_2} with frequency f_{s_2} and so on. One channel of the analog front-end electronics (AFE) serves at the moment for four sensors and consists of: two low noise single-ended charge amplifiers, low noise BP filter, analog mixer, 4th order low pass filter, 2nd order $\Delta\Sigma$ modulator with one-bit internal quantizer and multi-bit DACs built as analog FIR filter. The excitation signals are delivered to the sensors as a four low noise analog differential signals. The signal at the output of the charge amplifier, when all four sensors are present, is composed of four spectral components and their odd harmonics. The amplitude of each spectral line corresponds to one sensor and is proportional to the difference of the corresponding differential sensors capacitance and the amplitude of the corresponding excitation signal (1). Different sensors are driven with square-waves with slightly different frequencies. The amplitude of each spectral component carries the information about the difference ΔC of each sensor. The starting capacitance difference of each sensor is adjusted to be small during automatic calibration procedure at the beginning of the measurements. After adsorption of target molecules, the capacitance changes so the amplitude of the main spectral component changes. At the moment, one measurement channel can process signals from four differential sensors that might be functionalized differently. The idea behind the array of the sensors is that differently modified sensors show different responses to the target and other molecules in the air, producing a "signature" of the responses, which could improve the selectivity and sensitivity of the sensor system.

The difference in charges from each capacitive pair is transformed into the voltage using low noise charge amplifier through the use of excitation signals connected to the sensors. The frequencies are selected well above the flicker noise corner of the charge amplifier that is in the range of several 100 kHz for modern CMOS process [8]. Each sensor pair is driven with a differential square wave signal V_{s_i} producing charge amplifier output signal with amplitude given in (1), where $\Delta C = C_p - C_n$, V_s is the excitation voltage amplitude and C_f is the feedback capacitance of each amplifier. To remove unwanted components, the signal V_{cho} is band-pass filtered, amplified and multiplied with coherent square-wave signal with frequency f_m gener-

ated in the DSP. The spectrum after the passive mixer is a reach composition of sums and differences of all fundamental spectral components and their odd harmonics. Since amplified and filtered signals at the output of the band-pass filter contain main spectral components and attenuated higher harmonics, the analog mixer generates the differences and sums of the main spectral component frequencies and many high frequency spectral components.

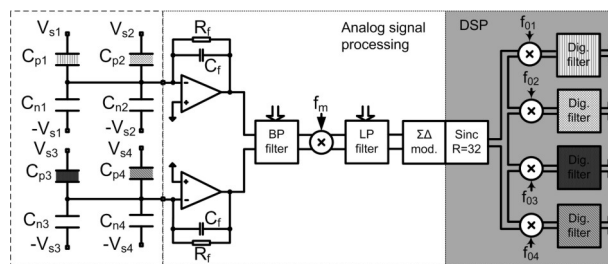


Figure 2: Block diagram of a complete sensor measurement system including 4 sensors, one measurement channel and corresponding DSP implemented in the FPGA.

The differences of the first harmonics happen at frequencies: $f_{oi} = f_{s_i} - f_m$ ($i=1\dots4$). They are amplified, while HF components with frequencies $f_{oi} = f_{s_i} + f_m$ ($i=1\dots4$) and other remains of higher harmonic signals mixing products are attenuated by programmable analog LP filter, which also adapts the level appropriate for the ADC. The frequencies f_{s_i} and f_m are selected in such a way that they are coherent [9], the components after mixing have different frequencies and the higher order products do not fall into the base-band. The composed signal is quantized using second order $\Sigma\text{-}\Delta$ modulator and a 3rd order sinc decimation filter with down-sampling ratio of 32. To speed up the detection process and avoid the problems of non-coherency, it is extremely important that all signals used for driving, mixing, down-sampling and timing of further filtering are strictly coherent, that is, the measurement period is a multiple of every f_{s_i} signal period generated in the circuit and that their ratios are prime numbers [9]. To be able to generate coherent signals, the decimation ratio is small in the first decimation stage; the remains of the out-of-band signals and shaped quantization noise are further filtered in each channel after digital mixing with f_{oi} as suggested in the DSP block on the right side of the block diagram shown on Fig. 2. The spectrum at the output of the first sinc filter consists of four spectral components at frequencies f_{o1} to f_{o4} with amplitudes proportional to the corresponding sensor capacitance difference and excitation signal amplitudes. This digital signal is then multiplied in four separated digital multipliers, each with a digital sine-wave with frequencies f_{o1} to f_{o4} translating corresponding signals to the DC. Each DC digital signal is then separately filtered in the DSP

to remove all remains of high frequency components. Each DC result is proportional to the difference of differential capacitances of each sensor and the excitation signal amplitude. The digital signal processing at DC is possible without compromising the signal quality. The bandwidth is reduced to approx. 10Hz in corresponding LP digital filter. The remains of the second mixing process are highly attenuated by appropriate positions of poles and zeroes of the digital LP filters. The results of all channels are transferred to the PC where further filtering and decimation takes place, reducing the effective bandwidth of each channel down to 1Hz or even more if necessary. The results are stored for further processing and presented on the screen of the PC.

Excitation signals transfer the information from slowly varying sensor capacitances, due to slow adsorption-desorption process, to the trans-impedance charge amplifier at frequencies that are well above the corner frequency of the flicker noise. The whole measurement system looks like a modified lock-in amplifier [10] using double mixing architecture to sense and amplify the signals at high frequencies and thus to avoid 1/f noise and DC offset effects in analog modules. All signals are coherent and selected in such a way that the ratio of f_{dec1}/f_{oi} is even integer. They are derived from one master clock with frequency $f_{clk}=25\text{MHz}$. Possible selection of the excitation signal frequencies for 4 sensors are: $f_{s1}=208.3\text{kHz}$, $f_{s2}=183.8\text{kHz}$, $f_{s3}=201.6\text{kHz}$ and $f_{s4}=189.3\text{kHz}$. Multiplying signals at the output of the BP filter with square-wave signal with frequency $f_m=195.3\text{kHz}$ generates the differences and sums of the first harmonics and also other higher harmonics that are LP filtered. The main spectral components after mixing are at frequencies: $f_{o1}=13.02\text{kHz}$, $f_{o2}=11.5\text{kHz}$, $f_{o3}=6.3\text{kHz}$ and $f_{o4}=5.9\text{kHz}$. This arrangement makes possible to use one analog channel and to avoid the DC offset and remaining 1/f noise effects in analog LP filters and the Σ - Δ modulator and makes possible to reduce the sampling frequency and thus reduced power consumption. It would also be possible to use HF chopping at each component at the expense of increased thermal noise effects, which means worse SnR and worse detection sensitivity. Since the adsorption-desorption process is slow process (in the range of several s), the offset voltage and 1/f noise would compromise the accuracy and the stability of the results if DC excitation signals would be used; the "DC" signal-processing happens in the DSP where no physical noise process can reduce the SnR of the results.

4 Circuit design

The decisive parameter regarding detection sensitivity of the measurement system is the S/N ratio at the

charge amplifier output. Fig. 3 shows simplified model of the charge amplifier with most important noise contributions, together with simplified model of one sensor and associated parasitic capacitances. The circuit implementation details of the charge opamps and the feedback resistors R_f are not shown because of the lack of space. The feedback capacitance of the charge amplifier is $C_f=1.5\text{pF}$, while small signal resistance of the feedback resistor is very high $R_f>10\text{G}\Omega$; the pole frequency of the charge amplifier is low enough not to influence the behavior of the spectral components and the noise contributions of the R_f is small enough around the lowest excitation signal frequency of 180kHz . The R_f is built as electronically tunable linear MOS resistor [11] that can be adjusted to have a very high resistance (bigger than $10\text{G}\Omega$). Each charge amplifier use differential, folded-cascode architecture with single ended output reaching input referred noise density of less than $15\text{nV}/\sqrt{\text{Hz}}$ at 200kHz . Two single ended amplifiers are used to be able to keep the potential of the sensing capacitors fixed. BP filter uses fully differential opamp with similar characteristics; its input signal is a difference of both charge amplifier signals. From this point on, the analog signal processing is fully differential. The most important noise contributors are: Noise V_{ndop} is the opamp noise and is multiplied with noise gain $G_{ndop} \cong (1 + \sum C_{vg}/C_f)$, where $\sum C_{vg}$ is the sum of all capacitors connected to the virtual ground of the opamp and C_f is the feedback capacitor of the charge amplifier; Input referred noise density of the BP filter is V_{ndBP} ; the noise density of the feedback resistor V_{ndRf} which is attenuated by its frequency transfer function $|H_{Rf}(\omega_s)|$; the noise density of the excitation signal sources V_{ndsp} and V_{ndsn} are multiplied by excitation signal gain $G_s \cong C_s/C_f$.

The SnR at the output of the charge amplifier can thus be calculated using (1) and (2).

$$V_{cho} \cong V_s \cdot (\Delta C/C_f) \quad (1)$$

$$V_{ndcho}^2(f_{oi}) \cong [V_{ndop} G_{nd,op}]^2 + V_{ndBP}^2 + 2 \cdot [V_{ndS} G_s]^2 + kTR_f \cdot |H_{Rf}(\omega_{oi})|^2 \quad (2)$$

Equation (1) estimates the signal at the charge amplifier output while (2) estimates the noise power density at the output of the charge amplifier around frequency f_{oi} assuming thermal noise approximation. The pole frequency formed by $C_f \cdot R_f$ must be much lower than the signal frequency f_{oi} to avoid attenuation and phase shift of the main spectral components. In addition, noise contributions of the R_f at low frequency are highly attenuated by the noise transfer function $|H_{Rf}(\omega_s)|$. The total noise power density at the output of the charge amplifier around signal frequency f_{oi}

is composed of all contributions. The biggest contribution is the charge amplifier noise density V_{ndop} multiplied by associated gain $G_{nd,op}$. Usually, contributions of all other noise sources in a low-noise measurement system are selected in such a way that they are smaller or equal to the charge amplifier contribution because this is the most difficult and expensive to reduce. The estimate of the detectable capacitance difference of one sensor can be calculated using (3) assuming: $S_nR=6dB$, noise bandwidth is $1Hz$, noise density of the opamp $V_{ndop}(f_{oi}) \leq 15nV/\sqrt{Hz}$, excitation signal amplitude $V_s = 4V$, $C_f = 1.5pF$ and the sum of all capacitors connected to the virtual ground of the opamp is equal to $\sum C_{vg} = 2.5pF$. Factor four in (3) comes from analogue and digital mixers (each contributes approx. $\sqrt{2}$ [12]), while another factor 2 comes from the peak to rms conversion (factor $\sqrt{2}$) and noise contributions from all other sources including the excitation signal generators. One can estimate minimum detectable capacitance change of the modified COMB capacitor caused by the adsorption of target molecules using (3); it is assumed that adsorbed molecules do not change the dielectric constant of the modified capacitor significantly.

$$\delta C \cong (4/V_s)V_{ndop} (C_f + \sum C_{vg}) = 0.06 [aF/\sqrt{Hz}] \quad (3)$$

$$d_m \cong (d_0 \cdot \delta C / (C_0)) = 120 \text{ fm} \quad (4)$$

Equation (4) gives the minimum detectable COMB capacitance distance change, which is 120 fm . This distance change is well below the thickness of the one layer of adsorbed target molecules, estimated to be approx. $0.5nm$ for the TNT [2].

5 System level modeling

The electronic measurement system was modeled using Matlab/Simulink. The concept, sensitivity, selectivity, and functionality of the analog and digital signal processing modules and sensors operation were checked. Most important non-ideal effects of the analog measurement channel modules were taken into considerations [14]: non-linearity, thermal noise, $1/f$ noise, kT/C noise, offset voltages, gains, gain bandwidth products, slew-rates, distortions, as well as a bit-true models of all DSP modules. The system level simulation results match very well to the circuit level simulation results and to the measurements of the real circuit.

The system level optimization and simulation is very efficient because of high level model. Fig. 4 shows simulated spectrum at the output of the $\Sigma\text{-}\Delta$ modulator for 2 sensors connected to the charge amplifier with ca-

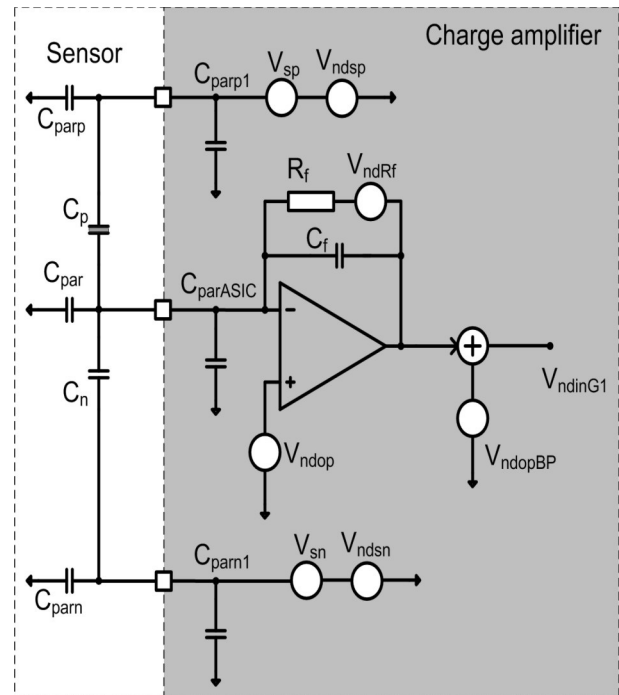


Figure 3: Noise sources of the input electronics of the AFE.

pacitance difference of $1fF$ for the first pair and $0.1fF$ for the second pair. The detection levels from system simulation results are very close to the estimates given in (3) and to the measured results. On Fig. 4, two main spectral components could be observed, each of them corresponding to associated sensor capacitance difference. The amplitude of the main spectral component at $11kHz$ is proportional to the capacitance difference of $1fF$ with $S_nR1=62.7dB$ in $200Hz$ band, while the S_nR2 is 20 dB smaller because of 10 times smaller capacitance difference. The result lead to the sensitivity of $0.037aF/\sqrt{Hz}$ (The noise contributions from the excitation signals are not included in the model, so the result is approx. $\sqrt{2}$ better than predicted by (3) and calculated from the measurements. High frequency components and shaped quantization noise are attenuated in the following decimation filters and DSP blocks, currently implemented on the FPGA. The digital part of the signal processing is also modeled in Simulink using bit-true models, so eventual finite word-length effects could be clearly observed. The Simulink models of the DSP blocks are used to synthesize the VHDL description of the DSP blocks directly from the models [15], while the analog part of the signal processing is designed "manually" using the information from the Simulink model as a specification for the circuit design parameters; in this way the total design time is drastically reduced, while increasing the reliability of the design.

6 Measurements

For laboratory measurements the PCB with System in Package (SiP) demonstrator was built as shown on the right part of Fig. 5. It is composed of the ASIC (left part of Fig. 5) and four differently modified differential sensors. During experiments, the package is covered with metal cover that seals the sensors completely. The cover has 2 holes; the mixtures of gases is delivered from the gas generator via one hole and expelled through another. In laboratory experiments the gas coming to the sensor surface is switched between dry N₂ gas and N₂ contaminated with TNT vapor molecules. At room temperature, the density of target molecules relative to the N₂ molecules is in a range of $X_{targ}=10^{-9}$ [2] dependent on the pressure, temperature etc.

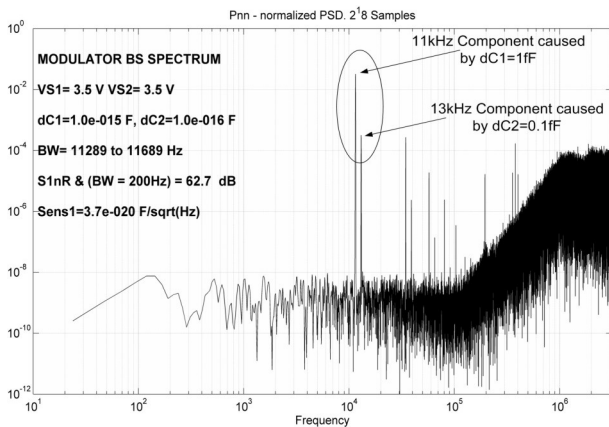


Figure 4: Spectrum at the output of the analog front-end for 2 sensors. Spectral line at 11 kHz is proportional to $\Delta C_1=1fF$, while spectral line at 13kHz is caused by $\Delta C_2=0.1fF$. Signal-to-noise ratio (SnR) is calculated for the main spectral line for 200Hz bandwidth, while Sensitivity Sens1 is valid for 1Hz band.

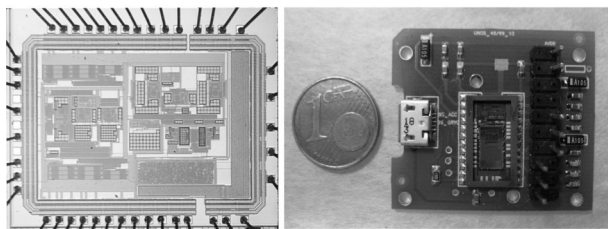


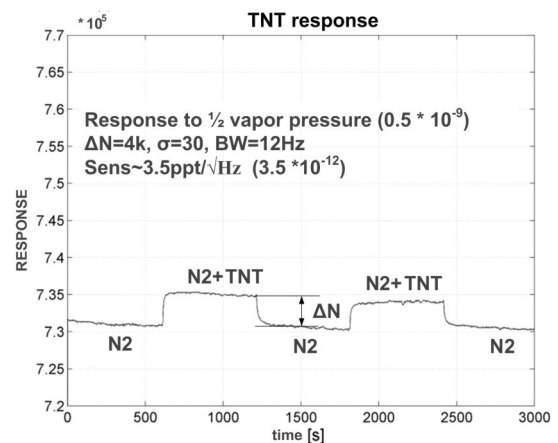
Figure 5: ASIC and SiP: (left) Photomicrograph of the ASIC in 0.25um BCD technology, (right): PCB with SiP (ASIC and 2 differential sensors).

Fig. 6 shows response of one measurement channel to the gas switched between N₂ and N₂ contaminated with TNT (estimated number of TNT molecules in the mixture is $0.5X_{targ}$). From Fig. 6 it is possible to estimate the normalized sensitivity S_{TNT} in 1 Hz band using (5), where: ΔN is the difference between two readings,

σ is the standard deviation of each reading (result), $BW=12Hz$ (after DSP filtering).

$$S_{TNT} \cong \frac{0.5 \cdot X_{targ} \cdot \sigma}{(\Delta N_{TNT} \sqrt{BW})} = \frac{3.5 \cdot 10^{-12}}{\sqrt{Hz}} \quad (5)$$

The lower level of the response on the y axis of Fig. 6 is proportional to the difference between capacitors after the calibration, while the change due to adsorbed molecules is proportional to ΔN . Long measurement times are produced by slow gas flow and big non-functional volume of the tubes. The sensitivity to the author's knowledge is still 2 to 3 orders of magnitude worse than the sensitivity of a dog's nose [3]. Currently, the selectivity measurements show that differently modified sensors provide different responses to the target and other molecules; this fact can be used to improve the selectivity. To the author's knowledge the system with comparable characteristics and using only available commercial technologies does not exist. Research papers regarding explosive vapor trace detec-



tion exists, for example [2], with comparable sensitivities but they use exotic technologies that are far away from possible industrialization.

Figure 6: Measured response of the N₂ and N₂ +TNT switching.

The first experimental measurements were performed also in the air for RDX vapors. The results are presented on Figure 7. Four differently modified sensors (APS, APHS, UPS, Reference) were exposed to the vapors of RDX in the air using a tube with topped RDX material. The tube on the left bottom picture is closed than in the middle it is opened, and on the right it is closed again. The sensors measurement system shows the screen of the PC with different responses of differently modified sensors as a function of time. We can see that differently modified sensors show different results and

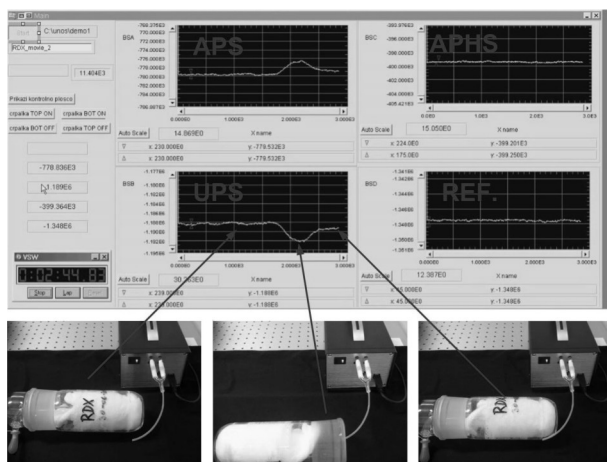


Figure 7: Measured responses of 4 differently modified sensors to RDX vapors in the air

no response is observed on reference sensor that is not modified at all.

7 Conclusions

Detecting vapor traces of different materials in the atmosphere is a potentially powerful method to reveal the presence of those materials. In this article, a miniature sensor detection system has been presented that is capable to detect vapors of different explosives. It is sensitive, selective, consumes a minimum amount of energy (10mA at 5 V), is very small and cheap to produce in large quantities and it is insensitive to mechanical influences. In laboratory environment, the response to TNT and RDX vapors has been measured. The detection levels for TNT of 3ppt and for RDX of 0.3ppthas been achieved. In the future, we plan to use large integrated array of differently modified sensors with improved individual sensitivities. This could lead to miniature, cheap and very selective detection system that could be massively deployed for detection of different hazardous molecules in the air. Measurement results in real environment are presented for RDX vapors. We have tested the sensitivity of the APS modified sensor to vapor traces of RDX with even better sensitivity than for TNT. Future work will be directed towards improving the sensitivity and the selectivity: changing the sensor geometry, reducing the analog channel noise and the parasitic capacitances of the ASIC and the sensors, increasing the number of differently modified sensors in the array and applying signature analysis algorithms to the results. We could come closer to dog's nose sensitivity and selectivity by one to two orders of magnitude using suggested modified MEMS COMB sensors and standard modern CMOS technology.

Acknowledgments

The research was partially founded by CoE NAMASTE and partly by Ministry of defense of the Republic of Slovenia.

References

1. Anja Boisen, Søren Dohn, Stephan Sylvest Keller, Silvan Schmid and Maria Tenje, "Cantilever-like Micromechanical Sensors," Rep. Prog. Phys., vol. 74, Feb. 2011.
2. J.Chen, P. Xu and X.Li, "Self-assembling Siloxane Bilayer Directly on SiO₂ Surface of Micro-Cantilevers for Long-Term Highly Repeatable Sensing to Trace Explosives," IOP Science Nanotechnology, vol. 21, Jun. 2010.
3. D. Strle, B. Štefane, U. Nahtigal, E. Zupanič, F Požgan, I. Kvasič, M. Maček, J. Trontelj, I. Muševič, "Surface-functionalized COMB capacitive sensors and CMOS electronics for vapor trace detection of explosives," *IEEE sens. j.*, May 2012, vol. 12, no. 5, pp. 1048-1057.
4. J.C. Love, L.A. Estroff, J.K. Kriebel, R.G. nuzzo, G.M. Whitesides, "Self-Assembled Monolayers of Thiolates on Metals as a Form of Nano-Technology," *Chem. Rev.*, 2005, 105, 1103-1169.
5. G. Ashkenasy, D. Cahen, R. Cohen, A. Shanzer, A. Vilan, "Molecular Engineering of Semiconductor Surfaces and Devices," *Acc. Chem. Res.* Vol. 35, No. 2, Feb 2002.
6. S. Fiorilli, et. al, " Vapor-phase self-assembled monolayers of aminosilane on plasma-activated silicon substrates," *Jour. Of Colloidal and Interface Science*, 2008, vol. 321, pp. 235-241.
7. Z. Peiji, W. Dwight, "Electrostatic Characteristics of Tether Atoms in Connecting Organic Molecules to the Surface of Silicon," *Applied Physical Letters*, vol. 91, nu. 6, Aug. 2007.
8. D. Šiprak, M. Tiebout, N. Yanolla, P. Baumgartner, C. Fienga, "Noise Reduction in CMOS Circuits Through Switched Gate and Forward Substrate Bias," *IEEE JSSC*, vol. 44, No. 7, July 2009.
9. M. Burns, G. W. Roberts, "An Introduction to Mixed-Signal IC Test and Measurement," Oxford university press, New York 2001.
10. M. Tavakoli, R. Sarpeshkar, "An Offset Cancellation Low Noise Lock in Architecture for Capacitive Sensing," *IEEE JSSC*, vol. 38, No. 2, Feb. 2003.
11. K. H. Wee and R. Sarpeshkar, "An Electronically Tunable Linear or Nonlinear MOS resistor," *IEEE Tr. CAS I.*, vol. 55, no. 9, Oct. 2008.
12. S. Chehrazi, A. Mirzaei, A.A. Abidi, "Noise in Current Commutating Passive FET Mixers," *IEEE Trans. On CAS. I.* Vol. 57, No. 2, Feb. 2010.

13. R. G. Vogt, "How sensitive is a Nose, "Science's STKE, vol. 322, Febr. 2006.
14. D. Strle, "Mixed-Signal Circuits Modeling and Simulations Using Matlab," Engineering education and research using MATLAB, In-Tech: 2011, pp. 113-147.
15. D. Raic, D. Strle, "Advanced CIC decimator modeling with HDL conversion in mind", Internal report, 2013.

Arrived: 28. 10. 2013

Accepted: 08. 11. 2013